BIOCHEMISTRY
including biophysical chemistry & molecular biology

Article

pubs.acs.org/biochemistry

Insights into the Structure of Intrastrand Cross-Link DNA Lesion-Containing Oligonucleotides: G[8−5m]T and G[8−5]C from Molecular Dynamics Simulations

Elise Dumont,*[,†] Tomáš Dršata,[‡] Célia Fonseca Guerra,[§] and Filip Lankaš*[,‡]

[†]Laboratoire de Chimie, UMR 5182 CNRS, École Normale Supérieure de Lyon, 46, allée d'Italie, 69364 Lyon Cedex 07, France

[‡]Institute of Organic Chemistry and Biochemistry, Academy of Sciences of the Czech Republic, Flemingovo nám. 2, 166 10 Praha 6, Czech Republic

[§]Department of Theoretical Chemistry and Amsterdam Center for Multiscale Modeling, VU University Amsterdam, De Boelelaan 1083, NL-1081 HV Amsterdam, The Netherlands

S *Supporting Information*

ABSTRACT: Oxidatively generated complex DNA lesions occur more rarely than single-nucleotide defects, yet they play an important role in carcinogenesis and aging diseases because they have proved to be more mutagenic than simple lesions. Whereas their formation pathways are rather well understood, the field suffers from the absence of structural data that are crucial for interpreting the lack of repair. No experimental structures are available for oligonucleotides featuring such a lesion. Hence, the detailed structural basis of such damaged duplexes has remained elusive. We propose the use of explicit solvent molecular dynamics simulations to build up damaged oligonucleotides containing two intrastrand cross-link defects, namely, the guanine−thymine and guanine−cytosine defects. Each of these lesions, G[8−5m]T and G[8−5]C, is placed in the middle of a dodecameric sequence, which undergoes an important structural rearrangement that we monitor and analyze. In both duplexes, the structural evolution is dictated by the more favorable stacking of guanine G6, which aims to restore π-stacking with the 3′ purine nucleobase. Subsequently, transient formation of hydrogen bonds with a strand shifting is observed. Our simulations are combined with density functional theory to rationalize the structural evolution. We report converging computational evidence that the G[8−5m]T- and G[8−5]C-containing stuctures evolve toward "abasic-like" duplexes, with a stabilization of the interstrand pairing noncovalent interactions. Meanwhile, both lesions restore B-helicity within tens of nanoseconds. The identification of plausible structures characterizes the last hydrogen abstraction step toward the formation of such defects as a non-innocent chemical reaction.

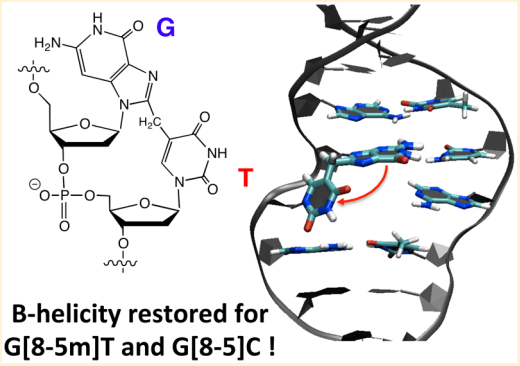

The constant exposure of biomolecules to free radicals (oxidative stress) triggers a number of damage processes that are more and more satisfactorily and exhaustively established. The elucidation of oxidatively generated defects is crucially important especially for DNA,[1] for which a lack of repair will result in genotoxicity. A family of DNA lesions with particularly important implications has emerged rather recently.[2] They feature two covalently tethered nucleobases, more precisely a purine−pyrimidine association. Measurements of formation yields for a series of purine−pyrimidine oxidatively generated cross-links (OCLs),[3] combined with theoretical calculations,[4,5] delineate some rules for understanding the formation of such defects. The first trend is that they involve preferentially a 5′ guanine. The three-step pathway leading to guanine−thymine and guanine−cytosine defects, depicted in Figure 1, is rather well understood. They are denoted G[8−5m]T and G[8−5]C, respectively, referring to the atomic positions implicated in the internucleobase cross-linkage. It is established that the formation of the guanine−thymine OCL is favored, with a formation yield of 0.050 lesion per 10^9 nucleotides per gray versus 0.035 for the guanine−cytosine moiety.[6] This is traced back to a higher B-helical distortion, as G[8−5]C does not present a methylene spacer.[7]

Such OCLs have been identified not only *in vitro* but also in cellular DNA.[6] Data on their repair have only recently been put forward,[8] and a firm structural basis for a more sound view of repair processes is lacking. Indeed, an in-depth understanding of the photolesion recognition and excision processes has been based on the X-ray structure of protein−DNA complexes caught in the act, which has highlighted the role of the bend angle induced by the cyclization process. In the same way, one seeks structural information about the way by which a B-DNA

Received: September 12, 2014
Revised: January 14, 2015
Published: January 20, 2015

DOI: 10.1021/bi501157v
Biochemistry 2015, 54, 1259−1267

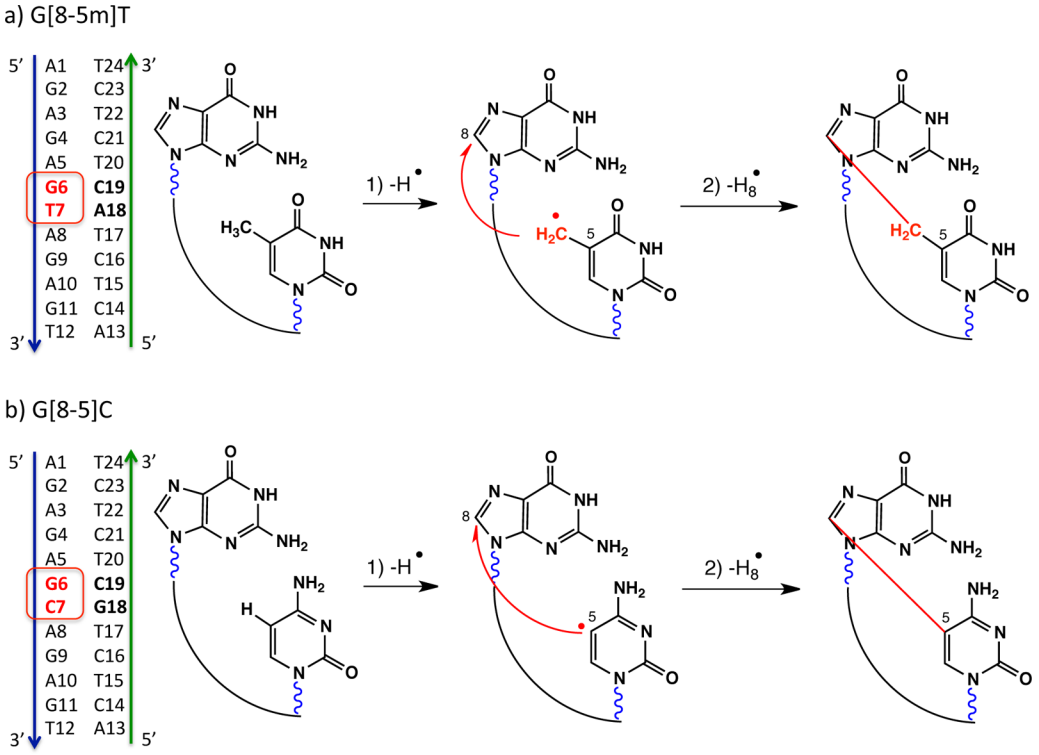

Figure 1. Dodecameric double-stranded sequences investigated in this study. Three-step pathways leading to the formation of G[8−5m]T and G[8−5]C cross-link lesions. They differ structurally in the nature of the covalent bridge tethering the purine and pyrimidine bases. We address the structural distortion they induce as placed in the center of a dodecameric sequence representative of B-DNA, after the departure of H8.

oligonucleotide will host an OCL lesion. It is surmised that having one versus two carbon−carbon linkages likely results in a very different structural outcome. This could be the reason why OCLs are much more refractory to repair than cyclobutane pyrimidine dimers, but no repair enzyme (NER or BER) has yet been caught in the act of detecting or excising an OCL. Thermal measurements have reported overall destabilization free energies of 3.6 kcal mol^{-1}[9] and 4.0 kcal mol^{-1}[10] for G[8−5m]T and G[8−5]C, respectively, embedded in the middle of a dodecamer, and with respect to the undamaged corresponding oligonucleotide. These values are significantly higher than the value for a *cis,syn*-cyclobutane pyrimidine dimer (1.5 kcal mol^{-1}[11]): this confirms the hypothesis of a very different structural outcome. These values are correlated to the potential of the lesions as substrates for UvrA binding.[9] In addition to this single energy measurement that reflects a structural deviation, a more detailed picture of the B-helix distortion is sought. It is established as a primary recognition factor.[12] The ∼2 Å shrinkage clearly affects the plane-to-plane angle between the covalently tethered pyrimidine and the guanine, as they can no longer be π-stacked. It may also modify the initial Watson−Crick pairing with the complementary nucleobases and alter the characteristic B-helix conformation, including the global bending angle.

In the absence of nuclear magnetic resonance or X-ray structures of OCL-containing oligonucleotides, we set out to investigate the structure, dynamics, and interactions of two dodecamers that feature a G[8−5m]T or G[8−5]C lesion embedded in the middle of the sequence (see Figure 1). One of us has recently focused on the formation of these two lesions[7] in exactly the same sequence, which is stable enough to be considered here as a realistic B-DNA environment. Because in that study we described a reaction, our modeling relied on a hybrid Car−Parrinello molecular dynamics density functional theory (DFT)/MM−MD scheme. However, typical time scales that such simulations can afford (100 ps in our case) remain too limited to provide a faithful description of the subsequent structural dynamics. To gain a clear picture and dramatically enhance sampling, and as no electronic phenomena come into play at this stage, an explicit solvent molecular dynamics (MD) simulation[13,14] offers a more reliable approach. It has been applied to carcinogenic agents,[15] but the view of oxidatively generated DNA coss-links has not gone beyond molecular models.[16] In Methods, we describe the force field parametrization we used for the cross-linked guanine−thymine and guanine−cytosine defects. The force field is then employed to perform MD simulations of the two OCL-containing dodecamers. We analyze the structural consequences of the OCL and, in particular, derive the global bending angle, which is known as a key feature for recognition and binding to repair enzymes.[17]

METHODS

Here we briefly summarize the methods employed in our study. More details are provided in the Supporting Information. All classical molecular dynamics simulations were performed using the Amber12 suite of programs.[18] Our starting structures featuring OCLs were taken at the end of a hybrid quantum mechanics−molecular mechanics reactive trajectory.[19] We chose to study the same sequence to delineate a comparison with the QM/MM−MD structures, and our study hence stresses the pitfalls arising from a lack of sampling (inherent to the cost of density functional calculations).

The parameters for the G[8−5]C and G[8−5m]T cross-link lesions were kept identical for the parts inherent to a single

DOI: 10.1021/bi501157v
Biochemistry 2015, 54, 1259−1267

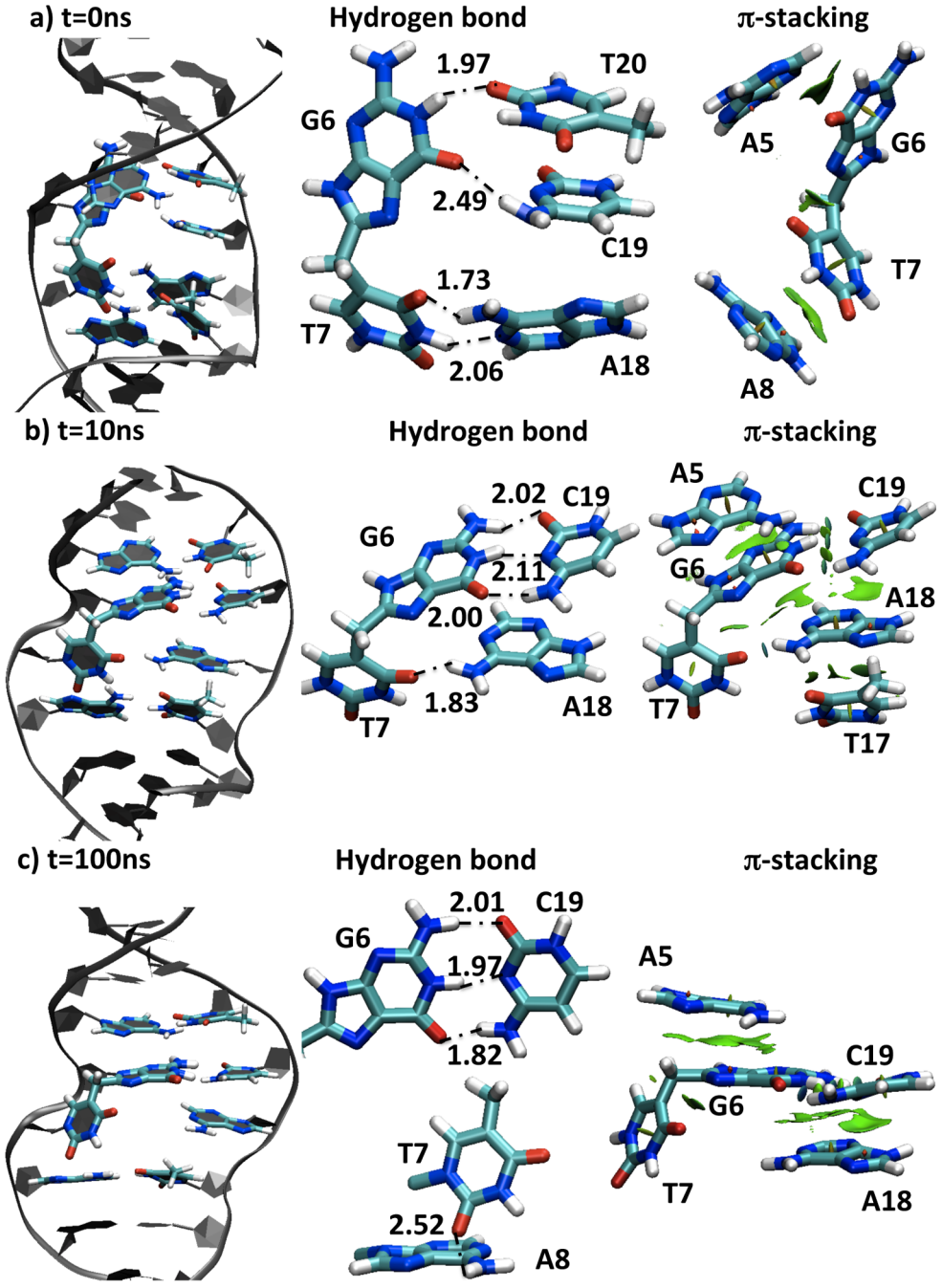

Figure 2. Cartoon representations of the G[8−5m]T lesion and its surrounding bases in the DNA duplex (a) at the beginning, (b) after 10 ns, and (c) at the end of the 100 ns MD trajectory. The blue and green NCI isodensities (the isovalue is 0.5 au, for a density cutoff of 0.1 au) reflect the presence of noncovalent interactions (HB and dispersion, respectively). Distances are given in angstroms.

nucleobase. The bonded force field parameters were taken from the Generalized Amber Force Field (GAFF),[20] and the ff99bsc0 force field, the best currently available for modeling B-DNA,[21] was used. Special care was taken to describe the guanine−thymine and guanine−cytosine C8···mC5 or C8···C5 linkages: C8 was set up as CT. Atomic charges were assigned using the restrained electrostatic potential (RESP) protocol[22] and are listed in Table S1 of the Supporting Information.

The two macromolecules were first neutralized using 22 potassium ions and then explicitly solvated using TIP3P water molecules in a periodic box of 70 Å × 71 Å × 66 Å Long-range interactions were calculated with the particle mesh Ewald (PME) method. The SHAKE algorithm was used to constrain bonds involving hydrogen atoms. The temperature was controlled using Langevin dynamics with a collision frequency of 1 ps^{-1}. A time step of 2 fs was used, and snapshots were taken every 2 ps. A series of minimization and MD runs were performed to equilibrate the system (see the Supporting Information). A production run of 100 ns was then conducted for each duplex. This simulation time was sufficient to identify key differences betweeen the conformational dynamics of G[8−5m]T- and G[8−5]C-containing duplexes.

The intra-base pair and inter-base pair (or step) coordinates and the orthonormal frames attached to DNA bases were computed using 3DNA.[23] The normal vectors of the G, T, and C planes within the lesion were defined using three atoms

DOI: 10.1021/bi501157v
Biochemistry 2015, 54, 1259−1267

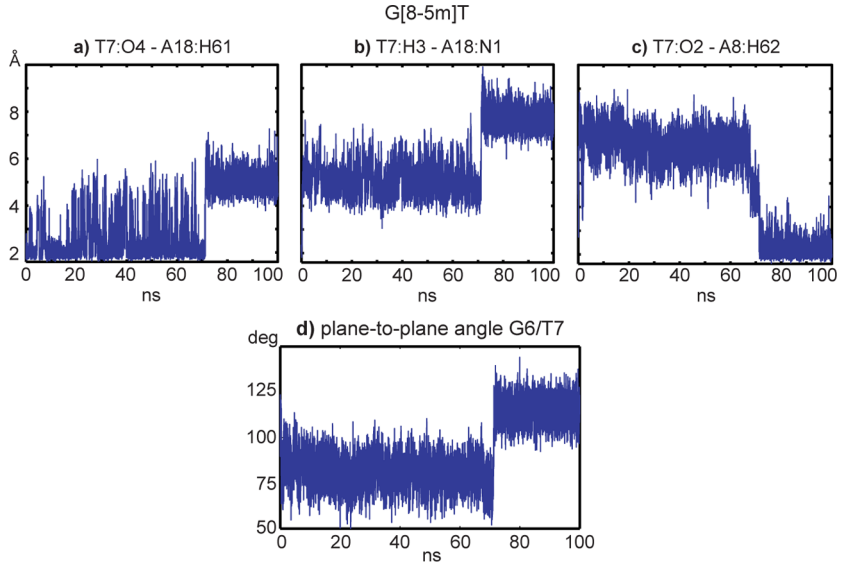

Figure 3. Evolution of the three distances corresponding to the hydrogen bond network between T7 and A8 or between T7 and A18 for the G[8−5m]T-containing duplex, and of the plane-to-plane angle $\phi^{G6/T7}$.

within each base (C2, C4, and C6 for all the bases). The magnitude and direction of global bending were measured as described previously.[24] Briefly, three global helical frames were defined in each oligomer, two at the ends and one in the middle. Each frame was obtained as the average of base-fixed frames of bases chosen in the helix. Bases in base pairs 2, 3, 10 and 11 were used for the end frames, and the middle frame was defined using bases in the two WC pairs flanking the lesion (bases A5, T20, A8, and T17). The bending magnitude was defined as the angle between the *z*-axes of the two end frames, and the direction was measured with respect to the middle frame.

Auxiliary DFT calculations were performed within the Amsterdam density functional (ADF) program[25] to quantify the strength of the Watson−Crick hydrogen bonding upstream and downstream from the T7-A19 base pair, i.e., between G6 and C19 and between A8 and T17 (or potentially any vicinal nucleobase). DFT has proven its reliability in that respect: we follow the procedure calibrated by Bickelhaupt and co-workers, relying on the BLYP functional, combining Becke's 88 exchange with the Lee−Yang−Parr correlation functional.[26,27] The dispersion correction was taken into account with the D3 version of Grimme's dispersion with Becke−Johnson damping (D3BJ[28]). This level of theory, in conjunction with the use of a TZ2P basis set, has proven to provide pairing interaction energies in very close agreement with the coupled-cluster CCSD(T) approach.[29] An energy decomposition analysis[30] is performed on a series of snapshots to evaluate the pairing interaction and its components in the vicinity of the lesion. At the same level of theory, a noncovalent interaction (NCI) analysis[31] is conducted to visualize the interactions taking place in the vicinity of the G[8−5m]T and G[8−5]C intrastrand cross-links. We note that this method is based on the electronic density gradient and Hessian principal values and allows the pictorial identification of dispersive interactions and π-stacking (green), hydrogen bonds (blue core), or steric clash (red). We do not explicitly include the backbone (sugar and phosphate) and perform DFT calculations in a pure QM formalism on the eight nucleobases, which are taken in the exact geometry of the B-helix conformation.

RESULTS AND DISCUSSION

Description of the G[8−5m]T-Containing Duplex. We first discuss the guanine−thymine lesion, which features a covalent carbon−carbon linkage that bridges the guanine G6[-H8] (C8 position) and the hydrogen-abstracted thymine T7[-H5m] in the dodecameric sequence we chose (Figure 1). This induces a local vertical shrinking of ∼2 Å that is initially accommodated within B-DNA notably by a deviation from the optimal π-stacking. The latter is captured in Figure 2a, where the structure obtained after equilibration (t = 0 ns) is represented. It can be measured by the plane-to-plane angle $\phi^{G6/T7}$ between G6 and T7, and this angle is close to 55° for the structure obtained at the end of a QM/MM−MD trajectory[19] but rapidly increases along the equilibration run to reach a value of 124° at the beginning of the MD production. It corresponds to a release of the steric strain, as the valence angle ∠(CCC) restores a value of 119° close to the equilibrium one (sp^3 hybridization of the methylene spacer).

Our simulations show that the opening motion associated with the increase in $\phi^{G6/T7}$ is not compatible with the conservation of a Watson−Crick pairing between G6 and C19 and between T7 and A18. The cartoon representation at t = 0 ns illustrates an almost complete disruption of the pairing between G6 and C19 (only a weak electrostatic interaction between G6 O6 and C19 H41 pertains at a distance of 2.49 Å). In that conformation, G6 is nevertheless stabilized by a transient offset hydrogen bond between one of the amino hydrogens, G6 H1, and T20 O2 (distance of 1.97 Å in Figure 2a). As a consequence, the A5:T20 pair deviates from planarity, and its Watson−Crick pairing is also weakened. The alteration of the B-helix conformation at t = 0 ns appears to affect mostly the G6-C19 and A5-T20 base pairs, as thymine T7 maintains a tight interaction mode with A18 via two hydrogen bonds with lengths of 1.73 and 2.06 Å.

However, this conformation very rapidly readapts (within <1 ns) as the guanine−thymine entity pivots to lead to a planar positioning of G6 with respect to A5. This allows the restoration of a nearly ideal Watson−Crick pairing between G6 and C19 (see the time evolutions in Figure 3) but also a π-stacking between A5 and G6. In particular, $\phi^{G6/T7}$ decreases

DOI: 10.1021/bi501157v
Biochemistry 2015, 54, 1259−1267

Table 1. Overall Interstrand Pairing Interaction Energies, $\Delta E^{pairing}$ (in kilocalories per mole), and Its Decomposition into Three Components, Evaluated at the DFT/BLYP-D3BJ/TZ2P Level of Theory[a]

snapshot	$\Delta E^{pairing}$	decomposition			
		Pauli + electrostatic = steric		orbital	dispersion
		G[8−5m]T			
reference undamaged DNA	−95.3	144.7	−125.4	19.3	−84.5	−30.1
t = 0 ns	−45.5	80.9	−65.0	15.9	−36.2	−25.2
t = 10 ns	−50.9	51.5	−53.5	−2.0	−30.7	−18.2
t = 100 ns	−66.5	95.8	−84.1	11.7	−51.8	−26.3
		G[8−5]C			
reference undamaged DNA	−102.8	160.7	−139.4	21.2	−91.0	−33.1
t = 0 ns	−56.2	99.3	−75.3	24.0	−47.9	−32.2
t = 10 ns	−61.9	96.8	−77.8	19.0	−49.1	−31.8
t = 100 ns	−65.9	78.8	−75.4	3.4	−44.1	−25.2

[a]The Pauli and electrostatic contributions add up to the steric contribution. Hydrogen bond stabilization corresponds to an orbital contribution.

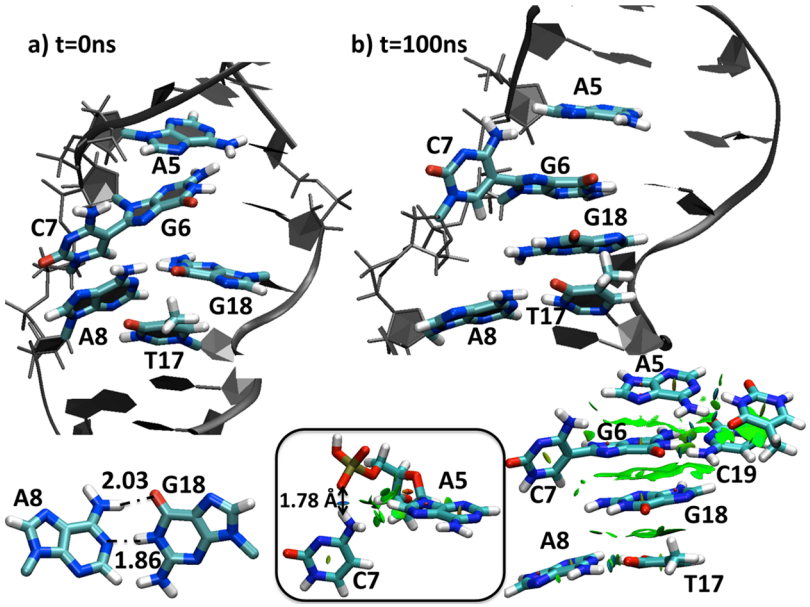

Figure 4. Cartoon representations of the G[8−5]C-containing duplex and the surrounding bases in the DNA duplex (a) at the beginning and (b) at the end of the 100 ns MD trajectory. More interstrand, offset dispersive interactions lead to a higher planarity among A5, G6, A18, and T17 can be seen on the NCI plot (green). The stable hydrogen bond between the amino group of C7 and the phosphate moiety linking A5 and G4 (blue isodensity; the isovalue is 0.5 au, for a density cutoff of 0.1 au) is represented in the inset.

from 124° within the first nanosecond and fluctuates around 81° (see Figure 3). This rotation of G6 of course inevitably impacts the spatial positioning of T7 because the two nucleobases are covalently tethered. Figure 2 shows that, at 10 ns, G6 has already moved to restore a tighter Watson−Crick interaction with C19, whereas the T7···A18 interaction is weakened with a single hydrogen bond between T7 O4 and A18 H61, at a distance of 1.83 Å for t = 10 ns, and with the loss of the NH···N interaction.

This structural evolution between the snapshots at t = 0 ns and t = 10 ns corresponds to a gain of pairing energy of 5.3 kcal mol^{-1} according to the energy decomposition analysis given in Table 1. This confirms that this structural reorientation of the guanine−thymine OCL within B-DNA is more favorable as G6 lies planar to A5: indeed, the disruption of the G6-C19 Watson−Crick interaction would induce a higher destabilization (25 kcal mol^{-1}) than the loss of T7-A18 pairing. We should also note that A5/G6 stacking is more stabilizing than T7/A8 stacking by 3 kcal mol^{-1}, such that both contributions tend to favor a π-stacked position of G6.

A sole hydrogen bond (T7 O4−A18 H61) is maintained up to 20 ns but then undergoes marked fluctuations until 70 ns, which can be seen from the time evolution of the HB distance given in Figure 3. After this transitory regime, T7 flips out and adopts an extrahelical position. At the same time, the plane-to-plane angle $\phi^{A5/G6}$ increases in a stepwise manner and starts to fluctuate around 114° (last graph, Figure 3). All interactions between T7 and A18 are thus lost, and the opposite A18 is left unpaired; however, this arrangement is very stable, until the end of the 100 ns trajectory. A cartoon representation at t = 100 ns (Figure 2c) illustrates this new conformation of the guanine−thymine OCL. The formation of a stable structure can be traced back to a nearly T-shape conformation that T7 adopts toward G6 and toward A8, which partially restores stabilizing London forces. The formation of an intrastrand hydrogen bond between T7 O2 and A8 H22 (amino group) also comes into play, which contributes to the orbital contribution; its time evolution is given in Figure 3 on the right side. It contributes to the anchoring of T7 and hence to the locking of the damaged oligonucleotide. One can also identify in panels b and c of

DOI: 10.1021/bi501157v
Biochemistry 2015, 54, 1259−1267

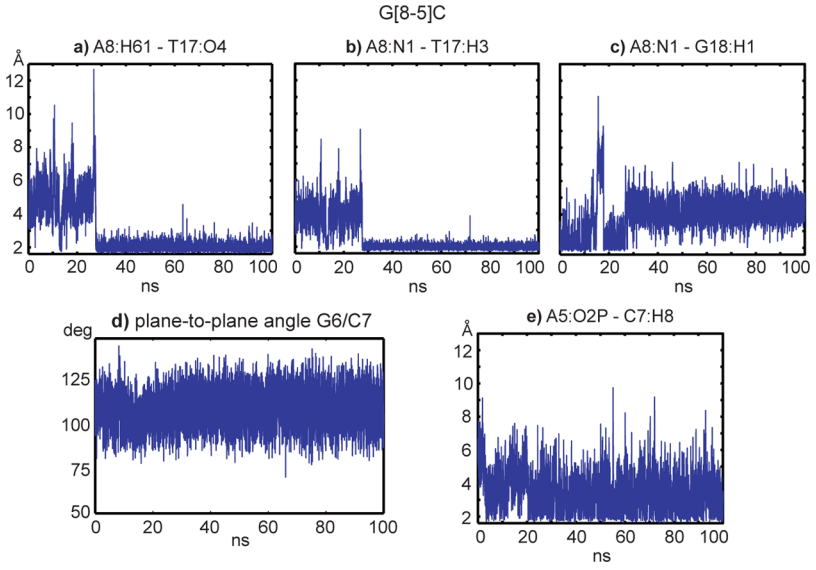

Figure 5. (a–c) Evolution of the three distances corresponding to the hydrogen bond network, between A8 and T17 or between A8 and G18 for the G[8–5]C-containing duplex. (d) Plane-to-plane angle $\phi^{G6/C7}$ that is stable during the production run. (e) Evolution of the HB distance between the phosphate group of A5 and the amino group of C7.

Figure 2 a transverse dispersive interaction between G6 and A18 (green regions of the NCI isodensities); it takes place as the structure behaves as an abasic site. We can note here that we recently identified a similar behavior for oligonucleotides featuring a C4′ abasic sites.[32]

In summary, the structural evolution of this G[8–5m]T-containing dodecamer obeys two rules: rearrange to re-form the G6-C19 pair, at the expense of the T7-A18 pair (because both cannot coexist in a stable manner because of the constraint of the methylene spacer), and concomitantly to restore B-helicity, an important feature that will be discussed in the last subsection of this manuscript, together with an energy decomposition analysis.

We have shown that the system evolves toward a well-characterized structure for the G[8–5m]T-containing oligonucleotide: we should note the importance of the neighboring nucleobases in the structural evolution of the dodecameric sequence we are considering here. The presence of a purine in position 5′ may trigger the preferential planar positionning of G6 via stacking interactions.

Description of the G[8–5]C-Containing Duplex. We now inspect the structural consequences of the analogous guanine–cytosine OCL, involving nucleobases G6 and C7, and taking place within the same dodecameric sequence. The only difference is the 18th residue, which is chosen to be a guanine, such that C7 is facing guanine G18 (see Figure 1).

The absence of a methylene spacer singles out G[8–5]C with respect to G[8–5m]T (and also most likely from G[8–5m]mC). Notably, the direct cross-link *a priori* should confer more rigidity to the system: this is reflected in our trajectories, as one observes two well-defined substates, whereas the G[8–5m]T lesion was found to exhibit more transient and oscillatory behavior. First, covalently bound cytosine C7 very rapidly adopts a linear arrangement. The latter is favored at least from the point of view of electronic structure after hydrogen abstraction of the G[8–5]C$^{\bullet}$ moeity, as the change in hybridization gives rise to an extended linear conformation, stabilized by aromaticity. Hence, the covalently tethered C7 pyrimidine hence rapidly adopts an extrahelical position.

Our simulations help us to identify the strategies the B-DNA environment develops to accommodate, and further stabilize, the G[8–5]C tandem lesion. For instance, A8 is found to stack with C7 at the beginning of the production run (t = 0 ns), as depicted in the cartoon representation given in Figure 4a. This spatial configuration of the duplex implies a local widening of the B-helix, because of the C7-G6···C19 triad. The orientation of this triad within the duplex leads to a mismatch of A8 with G18, instead of the canonical A8-T17 pairing situation. The interaction between A8 and G18 also implies two hydrogen bonds between C7 H21 and G18 O2, with lengths of 1.86 and 2.03 Å. They correspond to a rather strong hydrogen bond pattern, such that the G[8–5]C-containning oligonucleotide is stable in this conformation, up to 28 ns. Afterward, the duplex rearranges to adopt an alternative conformation, which is assigned, on the basis of the time evolutions given in Figure 5a–c for three hydrogen bond distances, to a disruption of A8-G18 pairing, whereas the Watson–Crick A8-T17 pairing is restored. This situation is depicted in the cartoon representation given in Figure 4b, for the final geometry obtained after simulation for 100 ns. Average distances and fluctuations are characteristic of a standard interaction, with a very limited weakening. In that interaction mode, the G18 nucleobase is no longer paired via hydrogen bonds but is nevertheless engaged in stabilizing, transverse dispersive interactions with G6 and T17. The latter can be seen from the NCI analysis (right side) and come into play to lock the duplex in a stable conformation. We note that this dispersion scheme is less pronounced for the guanine–thymine lesion.

We observe fewer fluctuations and less flexibility for the G[8–5]C system than for the G[8–5m]T analogue, a direct consequence of the absence of the methylene spacer. This rigidity implies that C7 can never be engaged in pairing interactions with a proximal nucleobase (such as A8). In contrast, we identify a relatively strong, stable HB interaction between the amino group of C7 and the phosphate moiety linking A5 and G4: a cartoon representation is given in Figure 4b, along with a time evolution of this HB distance in Figure 5e. This interaction, whose strength is estimated to be ∼4 kcal

DOI: 10.1021/bi501157v
Biochemistry 2015, 54, 1259–1267

mol^{-1} at the DFT level, drives an out-of-planarity conformation of the guanine−cytosine lesion, with a nearly orthogonal arrangement (110°), as can be seen from the comparison of panels a and b of Figure 4.

For both the conformers we identified, the G6-C19 Watson−Crick pair remains stable and the OCL-containing duplex tends to favor the stabilization caused by the purine moiety. This also corresponds to a more helical duplex, as we will discuss in the next subsection.

The Exclusion of the Pyrimidine Moiety Restores Stronger Interstrand Pairing Interaction and B-Helicity. We now inspect the effects of the lesion on the structure of the surrounding DNA. As soon as the stable conformation of the lesion has been reached [this happens at 70 ns for G[8−5m]T and at 28 ns for G[8−5]C (see above)], the whole oligomer becomes structurally stable. If one starts from that moment, WC pairs in the helices flanking the lesion remain intact, with the exception of short-lived transient fluctuation and the usual end effects (see discussion in the Supporting Information). The values of intra-base pair and step coordinates do not deviate from the range of B-DNA values. Thus, as soon as the lesion structure stabilizes, the DNA flanking the lesion retains its B-form.

The fact that one goes back to a more B-like structure can also be seen from the time evolution of the bend angle, given in panels a and b of Figure 6 for the G[8−5m]T and G[8−5]C lesions, respectively. The G[8−5m]T-containing oligonucleotide features an average angle of 57° between 0 and 65 ns, and after a reorganization regime (65−75 ns), it decreases to 26°. A similar, yet more rapid, evolution is found for the G[8−5]C-containing duplex: the bend angle is centered around 70° for the 3−25 ns part of the trajectory and then decreases to ∼45° (30−100 ns). Hence, and not unexpectedly, the absence of the -CH_2- spacer triggers a more drastic bending. The bending is always directed toward the minor groove in the oligomer center (bending direction of ∼180°). These values are comparable to those associated with photodimers such as the cyclobutane pyrimidine dimers that have been reported to induce bending of ∼30° and a widened minor groove,[33,34] yet they represent very distinct structures, as the photolesions do not adopt extrahelical positions. In contrast, our structure for the guanine−cytosine lesion is similar to that of the guanine−uracile OCL reported by Wetmore and co-workers, also obtained with an essentially similar methodology[35] (∼3 ns simulation). Our work reinforces the hypothesis of a contrasted situation of light-induced versus oxidatively generated defects, possibly in line with the lack of repair.

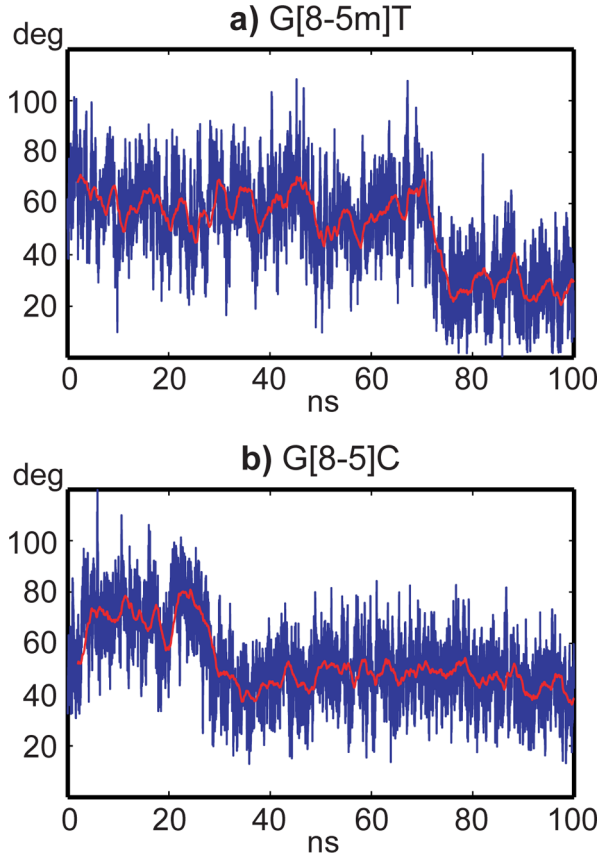

Figure 6. Time evolution of the bending angle along the classical trajectories.

To gain more quantitative insights and trace back the flipping observed for G[8−5m]T and G[8−5]C, we performed an energy decomposition analysis on six representative structures given in Figures 2 and 4. The series of quantum calculations that encompass eight nucleobases first confirms with no ambiguity a reinforced pairing. The gain in pairing energy accounts for 21 and 10 kcal mol^{-1} as we compare the first and final structures, respectively, in the second column of Table 1. This overall energetic stabilization constitutes with no ambiguity a driving force for the conformational changes leading to the final, less bent, structure of the OCL-containing lesions that are considered in this study. The data listed in Table 1 reveal in more detail the nature of the noncovalent interactions that take place and indicate two rather different behaviors for G[8−5m]T and G[8−5]C.

For the guanine−thymine defect, the initial interstrand pairing interaction between the A5···A8 and T17···T20 strands for the undamaged DNA accounts for −95.3 kcal mol^{-1}. One easily verifies that the hydrogen bonding contributions, of an orbital nature, are dominant [−84.5 kcal mol^{-1} (penultiame column of Table 1)]. At t = 0 ns, i.e., at the end of the equilibration regime, this canonical interstrand energy is decreased by almost 50 kcal mol^{-1}. The almost complete disruption of Watson−Crick interactions between G6 and C19 we observe at the beginning of the production run [t = 0 ns (Figure 2a)] would decrease the interstrand pairing $\Delta E^{\text{pairing}}$ by 25 kcal mol^{-1}. Then, this denotes that the Watson−Crick pairing is also weakened at other base pairs (e.g., the T7···A18 interaction).

The overall time evolution of the G[8−5]C-containing duplex similarly also features reinforced interstrand interactions along the classical trajectory: if one starts from a reference, undamaged value of −102.8 kcal mol^{-1}, the pairing energy is nearly halved at the beginning of the production run (t = 0 ns; $\Delta E^{\text{pairing}}$ = −56.2 kcal mol^{-1}). It is progressively reinforced as the damaged duplex relaxes, to reach −65.9 kcal mol^{-1} after classical MD for 100 ns. This time, the stabilization arises more directly from a release of steric interactions, for instance, between the two amino groups of A5 and G6, which can be seen in Figure 4a and accounts for ∼20 kcal mol^{-1} overall. Meanwhile, dispersion and orbital interactions are both weakened along the global rotation of the guanine−cytosine lesion, which results in an optimal placement of G6 with respect to A5 and C19. It is not surprising to find that the contribution of London forces is reduced (by ∼7 kcal mol^{-1})

DOI: 10.1021/bi501157v
Biochemistry 2015, 54, 1259−1267

because C7 is no longer in a stacking conformation with A8 or with another nucleobase in the final structure at t = 100 ns. The array of hydrogen bonds in panels a and b of Figure 4 is in agreement with a decrease quantified to ∼4 kcal mol^{-1} for the non-Watson pair.

CONCLUSIONS

While a clear view of the reactivity leading to OCLs within a DNA oligomer has progressively developed, a more pressing question is the quantification of the B-helical distortion upon formation of one carbon−carbon covalent linkage. In this work, we have extended a reactivity study by one of the authors to infer the structural consequences of OCL formation using explicit solvent molecular dynamics simulations, complemented by quantum chemistry calculations. We simulate representative DNA dodecamers containing OCLs that reach stable structures within 100 ns of simulation time.

We show that the structure of two OCLs fundamentally differs from that of photodimers, where two carbon−carbon single bonds are formed. They also differ from the 64PPs, a photoinduced lesion featuring a 6−4 cross-link between two thymines.[36] Our simulations reveal structural differences between G[8−5m]T and G[8−5]C, in spite of the experimental fact that the free energies of destabilization reported for the two lesions are close to each other (3.6 and 4.0 kcal mol^{-1}, respectively[9]). When covalently cross-linked to a guanine, thymine adopts a T-shape conformation, in contrast with cytosine that is stabilized in an extrahelical position. This structural difference may have specific implications for the recognition process.[37] Our simulations also unravel the specific role of vicinal nucleobases that come to stabilize the OCL-containing oligonucleotides. The extension of this work to other oligonucleotides would allow the probing and disentangling of possible sequence effects, notably the importance of the nucleobase in position 5′ of the intrastrand cross-link.

ASSOCIATED CONTENT

Supporting Information

Details of the computational procedure, supplementary Table S1, supplementary Figure S1, a cartoon representation of the estimation of the A5 O2P···C7 H8 hydrogen bond at t = 100 ns (Figure S2), and supplementary Figures S3−S5 for the full NCI cartoon representations of the G[8−5m]T-containing oligonucleotide. This material is available free of charge via the Internet at http://pubs.acs.org.

AUTHOR INFORMATION

Corresponding Authors

*E-mail: elise.dumont@ens-lyon.fr. Phone: +33 (0)4 72 72 88 46. Fax: +33 (0) 4 72 72 88 60.

*E-mail: filip.lankas@uochb.cas.cz. Phone: +420 220 410 319. Fax: +420 220 410 320.

Funding

This work was performed within the framework of the LABEX PRIMES (ANR-11-LABX-0063) of Université de Lyon, within the program "Investissements d'Avenir" (ANR-11-IDEX-0007) operated by the French National Research Agency (ANR). Calculations were performed using the local HPC resources of PSMN at ENS-Lyon. T.D. and F.L. were supported by the Grant Agency of the Czech Republic (14-21893S) and by the Academy of Sciences of the Czech Republic (RVO61388963).

Notes

The authors declare no competing financial interest.

REFERENCES

(1) Cooke, M. S., Evans, M. D., Dizdaroglu, M., and Lunec, J. (2003) Oxidative DNA damage: Mechanisms, mutation, and disease. *FASEB J. 17*, 1195−1214.

(2) Box, H. C., Budzinski, E. E., Dawidzik, J. B., Gobey, J. S., and Freund, H. G. (1997) Free Radical-Induced Tandem Base Damage in DNA Oligomers. *Free Radical Biol. Med. 23*, 1021−1030.

(3) Bellon, S., Ravanat, J.-L., Gasparutto, D., and Cadet, J. (2002) Cross-Linked Thymine-Purine Base Tandem Lesions: Synthesis, Characterization, and Measurement in γ-Irradiated Isolated DNA. *Chem. Res. Toxicol. 15*, 598−606.

(4) Xerri, B., Morell, C., Grand, A., Cadet, J., Cimino, P., and Barone, V. (2006) Radiation-induced formation of DNA intrastrand crosslinks between thymine and adenine bases: A theoretical approach. *Org. Biomol. Chem. 4*, 3986−3992.

(5) Labet, V., Morell, C., Grand, A., Cadet, J., Cimino, P., and Barone, V. (2008) Formation of cross-linked adducts between guanine and thymine mediated by hydroxyl radical and one-electron oxidation: A theoretical study. *Org. Biomol. Chem. 6*, 3300−3305.

(6) Hong, H., Cao, H., and Wang, Y. (2007) Formation and Genotoxicity of a Guanine−Cytosine Intrastrand Cross-Link Lesion *In Vivo*. *Nucleic Acids Res. 35*, 7118−7127.

(7) Patel, C., Garrec, J., Dupont, C., and Dumont, E. (2013) What Singles Out the G[8−5]C Intrastrand DNA Cross-Link? Mechanistic and Structural Insights from Quantum Mechanics/Molecular Mechanics Simulations. *Biochemistry 52*, 425−431.

(8) Wang, J., Cao, H., You, C., Yuan, B., Bahde, R., Gupta, S., Nishigori, C., Niedernhofer, L. J., Brooks, P. J., and Wang, Y. (2012) Endogenous formation and repair of oxidatively induced G[8−5m]T intrastrand cross-link lesion. *Nucleic Acids Res. 40*, 7368−7374.

(9) Gu, C., Zhang, Q., Yang, Z., Wang, Y., Zhou, Y., and Wang, Y. (2006) Recognition and Incision of Oxidative Intrastrand Cross-Link Lesions by UvrABC Nuclease. *Biochemistry 45*, 10739−10746.

(10) Gu, C., and Wang, Y. (2005) Thermodynamic and in Vitro Replication Studies of an Intrastrand G[8−5]C Cross-Link Lesion. *Biochemistry 44*, 8883−8889.

(11) Jing, Y., Taylor, J.-S., and Kao, J. F.-L. (1998) Thermodynamic and base-pairing studies of matched and mismatched DNA dodecamer duplexes containing cis-syn, (6−4) and Dewar photoproducts of TT. *Nucleic Acids Res. 26*, 3845−3853.

(12) Jain, V., Hilton, B., Lin, B., Patnaik, S., Liang, F., Darian, E., Zou, Y., MacKerell, A. D., and Cho, B. P. (2013) Unusual sequence effects on nucleotide excision repair of arylamine lesions: DNA bending/distortion as a primary recognition factor. *Nucleic Acids Res. 41*, 869−880.

(13) Ayadi, L., Coulombeau, C., and Lavery, R. (1999) Abasic sites in duplex DNA: Molecular modeling of sequence-dependent effects on conformation. *Biophys. J. 77*, 3218−3226.

(14) Radzimanowski, J., Dehez, F., Round, A., Bidon-Chanal, A., McSweeney, S., and Timmins, J. (2013) An 'open' structure of the RecOR complex supports ssDNA binding within the core of the complex. *Nucleic Acids Res. 41*, 7972−7986.

(15) Tomasi, J., Mennucci, B., and Cammi, R. (2003) Simulating Structural and Thermodynamic Properties of Carcinogen-Damaged DNA. *Biophys. J. 84*, 75020−75026.

(16) Price, N. E., Johnson, K. M., Wang, J., Fekry, M. I., Wang, Y., and Gates, K. S. (2014) Interstrand DNA-DNA Cross-Link Formation Between Adenine Residues and Abasic Sites in Duplex DNA. *J. Am. Chem. Soc. 136*, 3483−3490.

(17) Nagaich, A. K., Appella, E., and Harrington, R. E. (1997) DNA Bending Is Essential for the Site-specific Recognition of DNA Response Elements by the DNA Binding Domain of the Tumor Suppressor Protein p53. *J. Biol. Chem. 272*, 14842−14849.

(18) Case, D., et al. (2012) *AMBER 12*, University of California, San Francisco.

DOI: 10.1021/bi501157v
Biochemistry 2015, 54, 1259−1267

(19) Garrec, J., Patel, C., Rothlisberger, U., and Dumont, E. (2012) Insights into Intrastrand Cross-Link Lesions of DNA from QM/MM Molecular Dynamics Simulations. *J. Am. Chem. Soc. 134*, 2111−2119.
(20) Wang, J., Wolf, R. M., Caldwell, J. W., Kollman, P. A., and Case, D. A. (2004) Development and testing of a general amber force field. *J. Comput. Chem. 25*, 1157−1174.
(21) Zgarbova, M., Otyepka, M., Šponer, J., Mladek, A., Banáš, P., Cheatham, T. E., and Jurečka, P. (2011) Refinement of the Cornell et al. Nucleic Acids Force Field Based on Reference Quantum Chemical Calculations of Glycosidic Torsion Profiles. *J. Chem. Theory Comput. 7*, 2886−2902.
(22) Cieplak, P., Cornell, W. D., Bayly, C., and Kollman, P. A. (1995) Application of the multimolecule and multiconformational RESP methodology to biopolymers: Charge derivation for DNA, RNA, and proteins. *J. Comput. Chem. 16*, 1357−1377.
(23) Lu, X.-J., and Olson, W. K. (2008) 3DNA: A versatile, integrated software system for the analysis, rebuilding and visualization of three-dimensional nucleic-acid structures. *Nat. Protoc. 3*, 1213−1227.
(24) Lankaš, F., Spackova, N., Moakher, M., Enkhbayar, P., and Sponer, J. (2010) A measure of bending in nucleic acids structures applied to A-tract DNA. *Nucleic Acids Res. 38*, 3414−3422.
(25) te Velde, G., Bickelhaupt, F. M., Baerends, E. J., Fonseca Guerra, C., van Gisbergen, S. J. A., Snijders, J. G., and Ziegler, T. (2001) Chemistry with ADF. *J. Comput. Chem. 22*, 931−967.
(26) Fonseca Guerra, C., and Bickelhaupt, F. M. (2002) Orbital Interactions in Strong and Weak Hydrogen Bonds are Essential for DNA Replication. *Angew. Chem., Int. Ed. 41*, 2092−2095.
(27) van der Wijst, T., Guerra, C. F., Swart, M., and Bickelhaupt, F. M. (2006) Performance of various density functionals for the hydrogen bonds in DNA base pairs. *Chem. Phys. Lett. 426*, 415−421.
(28) Grimme, S., Ehrlich, S., and Goerigk, L. (2011) Effect of the damping function in dispersion corrected density functional theory. *J. Comput. Chem. 32*, 1456−1465.
(29) Riley, K. E., and Hobza, P. (2011) Noncovalent interactions in biochemistry. *Wiley Interdiscip. Rev.: Comput. Mol. Sci. 1*, 3−17.
(30) von Hopffgarten, M., and Frenking, G. (2012) Energy decomposition analysis. *Wiley Interdiscip. Rev.: Comput. Mol. Sci. 2*, 43−62.
(31) Johnson, E. R., Keinan, S., Mori-Sánchez, P., Contreras-García, J., Cohen, A. J., and Yang, W. (2010) Revealing Noncovalent Interactions. *J. Am. Chem. Soc. 132*, 6498−6506.
(32) Patel, C., Dršata, T., Lankaš, F., and Dumont, E. (2013) Structure, Dynamics, and Interactions of a C4′-Oxidized Abasic Site in DNA: A Concomitant Strand Scission Reverses Affinities. *Biochemistry 52*, 8115−8125.
(33) Husain, I., Griffith, J., and Sancar, A. (1988) Thymine dimers bend DNA. *Proc. Natl. Acad. Sci. U.S.A. 85*, 2558−2562.
(34) Park, H., Zhang, K., Ren, Y., Nadji, S., Sinha, N., Taylor, J.-S., and Kang, C. (2002) Crystal structure of a DNA decamer containing a cis-syn thymine dimer. *Proc. Natl. Acad. Sci. U.S.A. 99*, 15965−15970.
(35) Churchill, C. D. M., Eriksson, L. A., and Wetmore, S. D. (2011) Formation Mechanism and Structure of a Guanine-Uracil DNA Intrastrand Cross-Link. *Chem. Res. Toxicol. 24*, 2189−2199.
(36) Lee, J.-H., Hwang, G.-S., and Choi, B.-S. (1999) Solution structure of a DNA decamer duplex containing the stable 3′ T-G base pair of the pyrimidine(6−4)pyrimidone photoproduct [(6−4) adduct]: Implications for the highly specific 3′ T → C transition of the (6−4) adduct. *Proc. Natl. Acad. Sci. U.S.A. 96*, 6632−6636.
(37) Fuxreiter, M., Luo, N., Jedlovszky, P., Simon, I., and Osman, R. (2002) Role of Base Flipping in Specific Recognition of Damaged DNA by Repair Enzymes. *J. Mol. Biol. 323*, 823−834.

DOI: 10.1021/bi501157v
Biochemistry 2015, 54, 1259−1267